



HAL
open science

Magnetic anisotropy quantification in steel fiber reinforced materials

Daniel Alabi, Anastassios Skarlatos, Kyle A. Riding, Christophe Reboud, J. B. Harvey

► **To cite this version:**

Daniel Alabi, Anastassios Skarlatos, Kyle A. Riding, Christophe Reboud, J. B. Harvey. Magnetic anisotropy quantification in steel fiber reinforced materials. *NDT & E International*, 2024, 141, pp.102995. 10.1016/j.ndteint.2023.102995 . cea-04387625

HAL Id: cea-04387625

<https://cea.hal.science/cea-04387625v1>

Submitted on 11 Jan 2024

HAL is a multi-disciplinary open access archive for the deposit and dissemination of scientific research documents, whether they are published or not. The documents may come from teaching and research institutions in France or abroad, or from public or private research centers.

L'archive ouverte pluridisciplinaire **HAL**, est destinée au dépôt et à la diffusion de documents scientifiques de niveau recherche, publiés ou non, émanant des établissements d'enseignement et de recherche français ou étrangers, des laboratoires publics ou privés.

Magnetic Anisotropy Quantification in Steel Fiber Reinforced Materials

DJ Alabi^a, A Skarlatos^b, KA Riding^c, C Reboud^b and JB Harley^a

^aElectrical and Computer Engineering department, University of Florida, Gainesville, US

^bUniversité Paris-Saclay, CEA, List, F-91120, Palaiseau, France

^cDepartment of Civil & Coastal Engineering, University of Florida, Gainesville, US

ARTICLE INFO

Keywords:

Magnetic Anisotropy

Resin

NDT

Steel fibers

ABSTRACT

Fiber reinforced composites have grown in popularity over last few decades. Among these, steel fiber reinforced materials such as ultra-high performance concrete (UHPC) have begun use in the construction industry. Such materials provide an advantage over conventional fabrication techniques due to higher compressive, flexural, and tensile strengths. Yet, one challenge with fiber reinforcement is presence of unintended alignment during fabrication, which may deviate the material's strength from its intended design. This anisotropy needs to be nondestructively quantified to validate the material design post-fabrication. While electromagnetic nondestructive testing sensors have been demonstrated for quantifying the characteristics of ferromagnetic fibers in a material, there has not been a robust study on quantifying anisotropy with such systems. In this work, we provide the fundamental theory and process for quantifying anisotropy in steel fiber reinforced resins using electromagnetic sensors, with our data achieving a 95% goodness-of-fit with our theoretical model, on average.

1. Introduction

Fiber reinforced composites, such as ultra-high performance concrete (UHPC), are a versatile and highly durable materials that is used when high compressive [1], tensile [2], and flexural [3] strengths are needed for a structure [4]. These strengths are often the direct effect of the addition of steel fibers [1]. Based on the mixing procedure, these steel fibers could be distributed in a particular direction or randomly oriented, lacking any particular alignment. The difference in these distributions can significantly change the mechanical properties [5]. As a result, unintended mechanical variations due to these non-uniform fiber distributions can have a negative impact for the strength and durability of the concrete. While electromagnetic nondestructive testing sensors have been demonstrated for quantifying the characteristics of such ferromagnetic fibers in a material, there has not been a robust study on quantifying anisotropy.

The standard method for testing such anisotropy is typically through destructive methods [6]. For example for concrete, the member is cut open in sections to study the orientation and distribution of the fibers within. The challenge with this method is that the concrete must be cored and then destroyed, which is expensive and negatively impacts the integrity of the structure. Hence, this approach is not desirable as a regular testing or monitoring strategy [6]. In the field of nondestructive testing [7], the gold standard for assessing fibers is x-ray computed tomography (CT)[8]. While the sample may still need to be cored, this method enables the specimen to be inspected without damage and visually verify the arrangement of the fibers within the specimen. This method has its own challenges. First, it is difficult/impossible to test large specimen since most CT systems have size limitations and are not field deployable [9]. Second, due to the

size limitation, only portions of the specimen can be scanned by taking cores from the specimen to be scanned [8]. Third, CT scanning is time-intensive and the subsequent processing can require even longer with current computing technologies [8].

Other nondestructive methods have been implemented to quantify steel fibers in structures, generally with a focus on fiber-reinforced concrete. Ultrasonic methods [10] are some of the most common. Ultrasonic pulse velocity [11, 12] methods quantify steel fibers using the relative speed of the ultrasonic signal through the material [7]. Ultrasonic tomography methods [13] estimate the magnitude of the speed from the reflected or transmitted wave to construct a pattern representing the arrangement of the steel fibers [14]. Other methods for quantifying the steel fibers include the electrical resistance tomography [15], where a map of the internal structure is made based on the resistance of the structure at multiple sensors. A combined electromagnetic and radar method has also been used to determine the overall quality of steel fiber reinforced structure [16], and similar methods have been proposed for ground penetrating radar [17]. The primary challenge with these methods is that they are often more sensitive to the material variabilities than the geometry of fibers or they require a large number of sensors, which would prohibitively difficult for field use

In this work, we use a field deployable electromagnetic nondestructive testing device with fast scan time to quantify the anisotropy in specimens containing steel fibers. Electromagnetic methods are a powerful nondestructive testing tool since they do not interact with the concrete aggregate. For example, previous work has used electromagnetic methods such as eddy current [18] to produce electric currents through coils and create a magnetic field that interacts with steel rebars in concrete to produce a counter-current that is picked up either by the same coil or a pickup coil [19]. This method is very robust for finding rebars or concrete cover but is limited in use because it is not very suitable for steel

*Corresponding author

**Principal corresponding author

ORCID(s):

fiber reinforced specimen owing to its typical operation in high frequencies [20].

There have been some works in literature that use an alternative electromagnetic method that is more suitable for steel fiber reinforced materials [21]. This alternative method uses low frequency, electromagnetic sensors that consist of an inductor that is usually made by wrapping magnetic wire around a soft ferrite core. This device is then placed on specimen that contains steel fibers. The interaction of the steel fibers with the device increases the inductance of the device because the steel fibers are ferromagnetic materials with high magnetic permeability μ [22]. This change in inductance is proportional to the volume of steel fibers in the specimen, as shown in literature [23].

Several attempts have been made in literature to quantify this anisotropy (steel fiber orientation) in steel fiber reinforced concrete specimen [24] [25]. In [6], the authors used an electromagnet wrapped around specimen to quantify the volume and orientation of the steel fibers. While this is a good method for quantifying steel fiber volume and orientation, it is not practical as the shape of the sensor will have to be conformed to each specimen that needs to be tested. In [26, 27, 28], the authors put steel fibers between layers of material to quantify the fiber orientation. While successful at quantifying the fibers, this literature has largely been observational with respect to characterizing anisotropy and has focused primarily on a small number of test cases. In addition, there has been minimal theory and validation in the expected output of these sensors in the presence of anisotropy.

In this work, we fill this gap by presenting electromagnetic theory that describes the expected measurements from layers of aligned steel fibers. We further validate this theory with an electromagnetic device, one that is based on inductance changes in an electromagnet, as in prior literature [26, 28]. We demonstrate our approach with steel fiber reinforced resin specimens, where the orientation of fibers can be visually observed without destructive techniques or x-ray CT. Resin is also chosen for the specimen because, like UHPC, it is paramagnetic [29]. This means the resin and concrete will behave similar in the presence of an external magnetic field.

We consider 12 different specimens, 6 of which contained randomly oriented fibers and the other half exhibiting various forms of preferential orientation. We test our electromagnetic sensor by taking inductance measurements of these specimen to determine anisotropy in the specimen. Overall, we achieve an average 95% goodness-of-fit between our data and the theoretical model.

2. Methodology

The method behind how the materials were selected and prepared are discussed in detail in this section. We provide a detailed material selection, preparation, and constituents that make up the individual specimen. We also provide the justification for the material selection and specimen choice. The material for the study was carried out using a resin mix

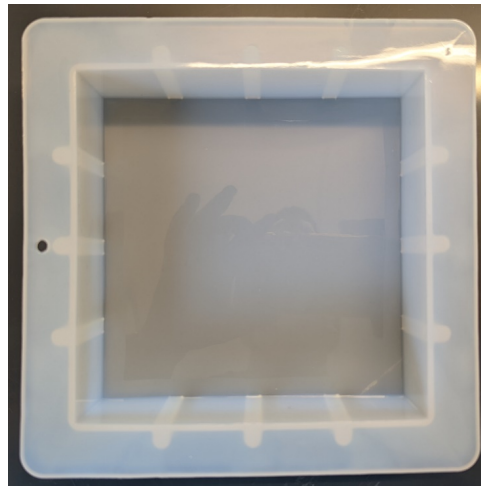


Figure 1: A 15.24 cm by 15.24 cm by 5.08 cm mold, used for making the specimen

with varying proportions of steel fibers added into the specimens.

2.1. Material Selection

There were several considerations made towards selecting the appropriate material to be used for the mock-ups. First was the fact that the material had to be paramagnetic so as to not affect the outcome of the magnetic readings. Second was the fact that the material must be easy to make and to allow the introduction of the steel fibers both in a random and oriented manner. The third consideration was the ability of the material to be transparent after it is made so that the insides of the specimen can be visually validated without resorting to x-ray scans or other scanning to observe fiber alignment.

Resin epoxy was the clear choice that meets all these requirements. Resin can be easily obtained and can be easily mixed and formed into various shapes and cast easily in molds. After deciding on the use of resins, the type of resin to use was further narrowed down based on the resin's curing time, viscosity, and temperature change. The curing time is important because resins that set too quickly would be difficult to introduce steel fibers into while resins that take too long to cure would be time wasting. The viscosity is important because steel fibers are dense, and it is important that the orientation pattern be intact while the resin is being poured into the mold. The temperature change was primarily chosen to ensure personnel safety.

Resoltech clear resin epoxy was selected as it meets all the requirements stated; it is clear, easy to make, curing time of about 2 hours, marketed as being UV resistant and easy to procure. The resin consists of two liquids; one with a relative density of 1.15 and the other with a density of 1.01, making a relative density of 1.10 for the mixture of the two liquids. This is still considerably lower than the relative density of the steel fibers, but with a 2 hour setting time, the mix can still be adequately controlled.

The mold for the mix is a white silicone mold with a



Figure 2: A 15 cm by 15 cm by 2.5 cm heat sink , used for aligning the fibers for the anisotropic specimen. It contains 22 grooves

square cross sectional area and dimensions 152.4 mm by 152.4 mm by 50.8 mm, shown in Figure 1. The silicone mold was chosen because of its flexibility, it helps with demolding the specimen without damaging either the specimen or the mold. It also makes the mold reusable for making several specimens without damage or permanently stained. For making the anisotropic specimen, an aluminium heat sink is used with dimensions 150 mm by 150 mm by 25 mm and contains 22 slits/grooves, as shown in Figure 2. These grooves are where the steel fibers for the anisotropic specimens are poured to align them before being placed in the mold to form the orientation in a particular direction.

2.2. Material preparation

Before the samples were made, the density of the steel fibers was calculated to ensure accuracy of the specimen mix. The density was calculated by first weighing a graduated 100 ml plastic measuring cup. Steel fibers were then placed in the graduated plastic measuring cup and weighed. The weight of the steel fibers was calculated as the difference between the two measurements. To calculate the volume of these fibers, water was poured in the graduated measuring cup and the volume was noted, the weighed steel fibers were then introduced into the measuring cup containing the water and the new volume was noted. The rise in water level (difference between the water levels) was then noted and recorded as the volume of the steel fibers. The density of the steel fibers was then calculated as

$$\text{density}_{\text{steel fibers}} = \frac{\text{mass}_{\text{steel fibers}}}{\text{volume}_{\text{steel fibers}}} \quad (1)$$

The density was calculated to be 8.95 g/cm³ against the expected reference value of 8.85 g/cm³. The density was then used to subsequently calculate all the steel fiber volume needed for each specimen mix.

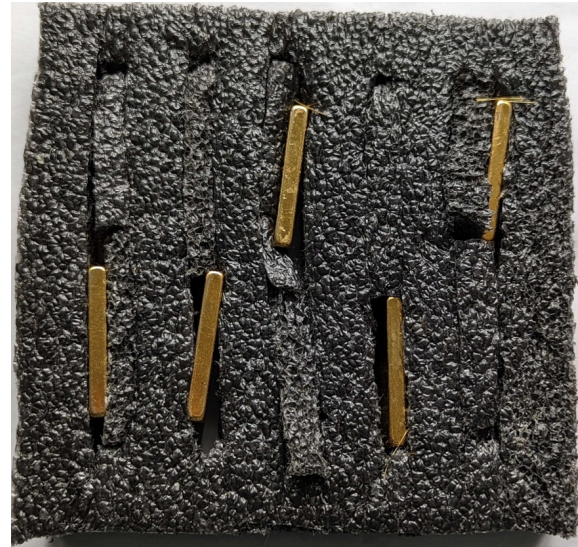


Figure 3: A custom-made magnetic stirrer to ensure proper randomization of the steel fibers for the isotropic specimen

The resin used has a mix ratio of 2 : 1 by volume and 60 : 40 by weight. We use a volume mix ratio in this work. The resin is mixed by volume and then poured into the mold, the steel fibers are weighed to account for the right percentage by volume (using the density calculations) and then poured into the mold. The steel fibers are stirred in by our custom-made mixer shown in Fig. 3. The stirrer consists of 5 magnets inserted into a packing Styrofoam in such a way that the fringing fields are outwards to enable stirring of the steel fibers. The stirring is to ensure a true randomization of the fibers, producing a nearly true homogeneous fiber mix.

For the preferentially oriented samples, the fibers are first weighed out, then poured into the grooves of the heat sink, ensuring that the fibers are as nearly evenly distributed in the grooves as much as possible. The heat sink is then covered with the mold, then flipped to ensure that the fibers align properly at the base of the mold. The resin is then poured into the mold with the the heat sink still in it to ensure that as the resin is flowing, it does not disrupt the alignment of the fibers. We do not use our custom stirrer for the preferentially oriented specimens because we do not want to randomize the mix. After the resin and steel fibers are poured into the mold, the mix is left to set. The heat sink is gently removed using tweezers to allow for little to no disruption of the steel fiber alignment as it is being removed. The mix is left to cure and set then the specimen is demolded and the process is repeated for other specimens.

2.3. Samples

In all, 12 resin samples were made. These samples include (note: all fiber percentages are by volume):

- Samples 1 & 2: Two randomly oriented, 1% fiber.
- Samples 3 & 4: Two randomly oriented, 2% fiber.
- Samples 5 & 6: Two randomly oriented, 4% fiber.

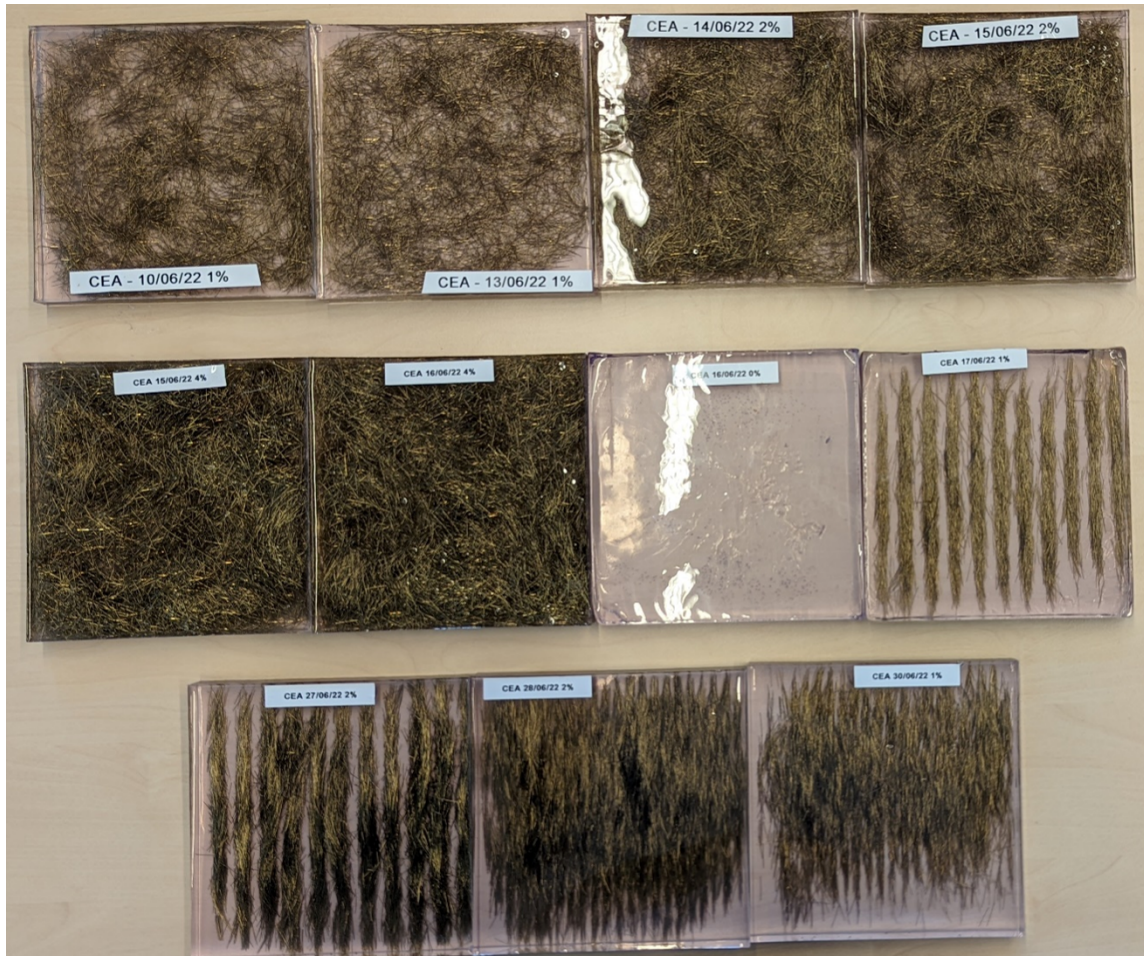


Figure 4: A collection of all the specimen placed side-by-side ranging from the randomly oriented to the preferentially oriented, and the control specimen

- Sample 7: One preferentially oriented, 1% fiber with the fibers concentrated and spaced about 5 mm apart.
- Sample 8: One preferentially oriented, 1% fiber with the fibers not spaced.
- Sample 9: One preferentially oriented, 2% fiber with the fibers concentrated and spaced about 5 mm apart.
- Sample 10: One preferentially oriented, 2% fiber with the fibers not spaced.
- Sample 11: One preferentially oriented, 2% fiber made cross-layered, with a 1% fibers on one half of it and another 1% fibers crossed directly on it.
- Sample 12: One control 0% fiber by volume.

The samples are shown in Fig. 4. The control sample was used to confirm our measurements and it is in agreement with measurements in the air. We do not otherwise show results from this sample.

3. Theory

This section details the theoretical basis of this work. We used an experimental method to test our hypothesis that



Figure 5: A cross-layered specimen showing the steel fibers in a cross-layered pattern

will be referred to as the inductance method. Magnetic permeability μ is the underlining factor of this experimental method. The magnetic permeability μ of a medium, is de-

defined as

$$\mu = \mu_0 \mu_r \quad (2)$$

where μ_r is the relative permeability of a medium, and μ_0 is the permeability of free space given as $4\pi \times 10^{-7}$ H/m. Magnetic permeability μ is defined as the ability of a material to form a magnetic field within itself when the material is under the influence of an applied external magnetic field. The steel fiber is a ferromagnetic material with a high permeability [29].

3.1. Inductance Method

Inductance is the ability of a conductor to resist the change in the electric current flowing through it. This property is highly dependent on the conductors permeability μ . The inductance L of a long solenoid (good example of an inductor) is given by the following relationship

$$L = \frac{\mu N^2 A}{l} \quad (3)$$

where L is the inductance, N is the number of coil turns, A is the area of the inductor, and l is the length of the inductor. In our case of a ferromagnetic yoke excited by a coil, (3) gives a good approximation of the coil inductance owing to the magnetic field guidance effect through the yoke core (the demagnetising field effect due to the free ferrite surfaces being neglected). Considering (3), we can see that with all other factors being the same, a change in μ will cause a corresponding change in the inductance, L of the medium. This means that in the presence of steel fibers that have very high μ , our inductance will also increase proportionally to the volume of the steel fibers present in the test specimen.

Magnetic circuit analysis [30] is a method that is used to model the flow of magnetic flux through magnetic loops. This magnetic circuit is analogous to the electric circuit, where the magnetomotive force (mmf) takes the place of the electromotive force (emf) which is the metaphoric force that is driving the circuit. The magnetic flux (or just simply flux, Φ), is the equivalent of the electric current, and the reluctance \mathcal{R} of the magnetic circuit is analogous to the resistance R of the electric circuit. The mmf of the circuit is related to the flux and the reluctance by

$$\text{mmf} = \Phi \mathcal{R} \quad (4)$$

which implies

$$\Phi = \frac{\text{mmf}}{\mathcal{R}} \quad (5)$$

The reluctance can be defined as

$$\mathcal{R} = \frac{l}{\mu_r \mu_0 A} = \frac{l}{\mu A} \quad (6)$$

where l is the length of the magnetic circuit, μ is the permeability of the medium, μ_r is the relative permeability of the medium, and μ_0 is the vacuum permeability given as $4\pi 10^{-7}$ H/m.

Taking into account the relation between the mmf and the coil driving current I

$$\text{mmf} = NI \quad (7)$$

and using Faraday's law, we arrive at the following relation for the coil inductance in the air

$$L_a = \frac{N^2}{\mathcal{R}_c + \mathcal{R}_a} \quad (8)$$

with \mathcal{R}_c being the reluctance of the coil with the ferrite core and \mathcal{R}_a being the air reluctance corresponding to the air gap between the yoke legs. Eq. (8) provides a better approximation for the free-space induction of the coil with the yoke since it takes into account the demagnetisation field through the \mathcal{R}_a . The respective relation with the yoke above the specimen is obtained by replacing \mathcal{R}_a with $\mathcal{R}_s = \mu_0 \mathcal{R}_a / \mu_s$, where μ_s stands for the specimen permeability (we ignore the air gap between the core and the specimen). Subtracting (8) from the corresponding relation above the specimen, we arrive to the following relation for the inductance change

$$\Delta L = \frac{N^2}{\mathcal{R}_c + \mathcal{R}_a} - \frac{N^2}{\mathcal{R}_c + \mathcal{R}_s} \quad (9)$$

$$= N^2 \frac{\mathcal{R}_a - \mathcal{R}_s}{(\mathcal{R}_c + \mathcal{R}_a)(\mathcal{R}_c + \mathcal{R}_s)} \quad (10)$$

which for high core and medium permeabilities $\mu_c \gg \mu_s \gg \mu_0$, becomes

$$\Delta L \approx \frac{N^2}{\mathcal{R}_s} = \frac{N^2}{l_a} \mu_s \quad (11)$$

(i.e., it is directly proportional to the specimen permeability variation μ_s).

This expression can be then extended to cover for the orientation by defining an angular dependence around the mean value of μ_s , defined by

$$\Delta L \approx \frac{N^2}{\mathcal{R}_s} = \frac{N^2}{l_a} (\mu_s (1 + \eta \cos(\omega\theta + \phi))) \quad (12)$$

In this expression, we refer to η as the anisotropic factor. This term satisfies $0 \leq \eta \leq 1$, where 0 represents no anisotropy. In addition, θ is the angle of inclination of the sensor (measured for 0 to 2π radians) and ω is the frequency of variation along this rotation. Finally, ϕ is the rotation of the anisotropy around the circle (i.e., $\omega\theta = -\phi$ is the angle of maximum inductance). Note that we are only able to observe orientations projected onto the two-dimensional plane that we can sense across. Hence, fibers oriented along the depth of a specimen should increase μ_s but not affect η .

4. Experimental Setup

Our inductor shown in Figure 7 contains 150 turns of 0.5 mm magnetic wire. It is wrapped around a ferrite core, has an inductance of 2.3 mH at 20 Hz, and a direct current

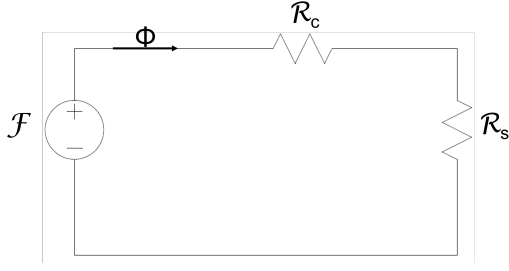


Figure 6: Setup showing magnetic circuit for the device in air. The F represents the magnetic force from the magnets which drives the flux Φ , the R_c is the reluctance of the core, and R_s represents the reluctance of air.



Figure 7: A magnetic sensor/inductor made with 150 turns of 0.5 mm magnetic wire wrapped around a U-shaped ferrite core.

(DC) resistance of 2.9Ω . The ferrite core measures 70 cm by 30 cm by 20 cm. This core was chosen because of its high permeability. Other work has discussed the impact of the core's geometry for similar results [31]. The inductance of our sensor was measured at 20 Hz. The approximate depth of penetration is 5 cm, as shown in prior empirical studies [31]. The relative permeability of the steel fibers in the specimen is given by the manufacturer as 100 while the relative permeability of the core is on the order of 1000 whereas the air relative permeability is approximately 1, which means that (12) makes a good approximation of the measured inductance variation.

We mixed the resin as described in the methodology section. The data was collected by placing the sensor on a 360° angle plot, as shown in Fig. 8, to enable accurate angular orientation. Note that the core shown in Fig. 8 is an illustrative example and is not representative of the core used in the experiments, which is shown in Fig. 7. The data was collected in 30° increments starting from 0° until 360° to ensure that we adequately capture the anisotropic angular de-

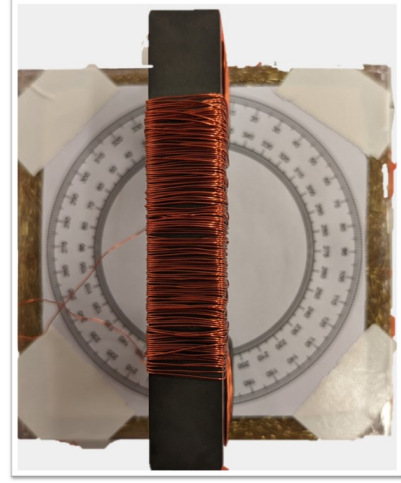


Figure 8: Specimen showing angle plots that are printed and pasted on each specimen that are used to measure the angular data accurately.

pendence. We connect the sensor data from a KEYSIGHT Impedance Analyzer E4990A. The sensor is placed in direct contact with the surface of the specimen at the desired angle marks and the reading is recorded. The procedure is repeated for all 12 samples.

We extract the result from the impedance analyzer onto a computer where data analysis is performed. We plot the average inductance measurements for both specimens of the 1, 2, and 4 fiber percentages against the inductance. We fit a linear line to it and take note of the intercept on the y-axis. This intercept is now taken as the baseline L_a , which consists of inductance from the air measurement and sensor. This baseline is then subtracted from the data to get ΔL , a reading based on the specimen's impedance properties only.

Note that while this study assesses a general mathematical relationship that is independent of specific application, the length (12 mm, on average), thickness (0.2 mm, on average), and density (1% to 3%) of the fibers used in this study are same as those used in steel fiber reinforced UHPC. In addition, both concrete and the resin used in this study are paramagnetic materials. The primary difference is that the resin was used to easily manipulate the orientation of the fibers and conduct the study.

5. Results and Discussion

This section details the results showing the anisotropy of the steel fibers in resin specimens. Table 1 summarizes all of our results of fitting our theoretical model in (12) with the measured data.

5.1. Randomly Oriented Fibers

We first show the results for specimen with randomly oriented fibers. The ideal isotropic result is a circle (relative to the angle of the sensor) with a fixed radius whose magnitude linearly increases with the increase in fiber percentage. Figures 9(a), 9(b), and 9(c) show the results of the 1%, 2%, and

4% specimens, respectively. Since each randomly oriented percentage has two specimens by fiber percentage, the results are shown along with their averages. Fig. 10 shows the average values of the randomly oriented specimens, the result shows a proportional increment in the inductance change with a corresponding increase in the fiber percentages.

We visually observe that there are slight anisotropy in the results, which can be attributed to differences arising from the fiber stirring process and the fact that the steel fibers usually have remnant magnetism that weakly aligns them along their length and results to some form of clumping. Overall, the results are relatively circular, particularly compared with the anisotropic samples discussed in the next subsection. In Table 1, the anisotropy factor η is consistently below 0.2 for these samples, well below η for the anisotropic samples. The average R^2 goodness-of-fit with our theoretical model is 0.93 for these samples.

5.2. Preferentially Oriented Fibers

Comparing the results for the preferentially oriented and the randomly oriented together, Fig. 11(a) shows the randomly oriented (averaged) specimens alongside the results of the preferentially oriented specimens with spaced and not spaced fibers. It can be observed from Figs. 11(a) and 11(b) that the inductance change for the samples without spacing is higher than that of the spaced, which in turn is higher than that of the randomly oriented samples along the primary axis. This may seem counterintuitive since the local densities of the fibers will be higher in the sample with spacing. However, the air gaps create magnetic flux leakage (not dissimilar to the that measured by a magnetic flux leakage sensor [32]) that reduces the overall flux and thereby reduces the sensor's inductance. Hence, the sensor is sensitive to non-uniform spatial fiber variability within the sample, although quantifying this dependency will require greater study.

The results for the preferentially oriented, spaced, and unspaced can be represented by a sinusoid fitted to the points. The result for the 2% preferentially oriented spaced specimen is shown in Fig. 12. When fit to sinusoid in (12), the result of the 2% preferentially oriented spaced specimen shows an average R^2 goodness-of-fit of 0.95, which indicates that the preferentially oriented spaced fits our mathematical model well.

5.3. Anisotropy Quantification

Table 1 illustrates that the samples with preferentially aligned (in a single direction) fibers have significantly larger anisotropy factors η than the samples with isotropic / randomly distributed fibers. The isotropic samples are consistently under 0.2 while the single-direction anisotropic samples are consistently about 0.4. The factor is not higher because the physical spread of the aligned fibers allows for magnetic flux in directions other than the aligned fiber direction. In addition, we observe that show the results of a measurement from both sides. We observe that for μ_s , the value generally increases linearly with fiber percent. This holds true even for the aligned specimens, where we see a

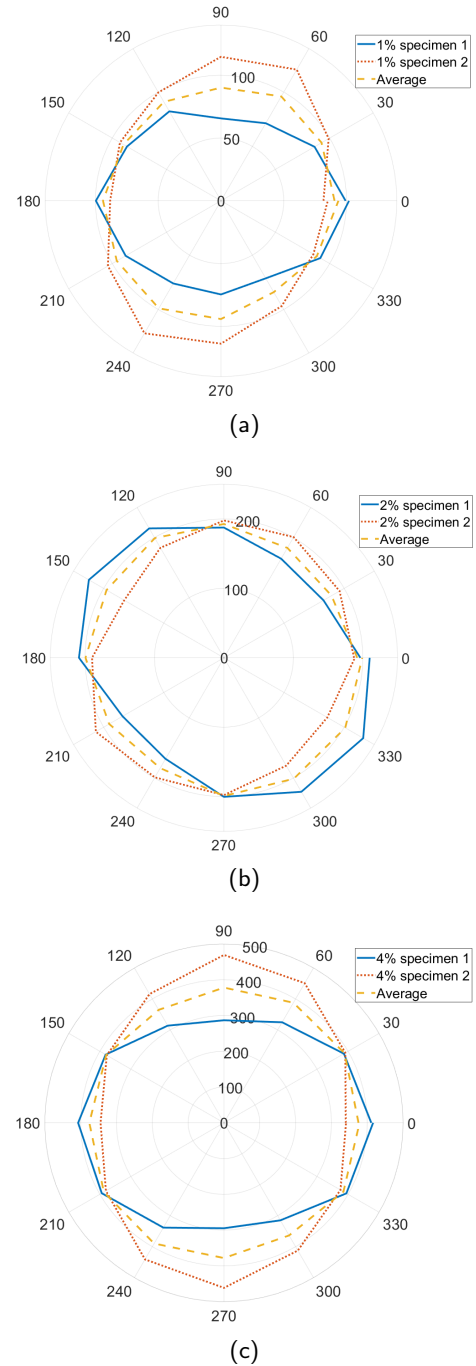


Figure 9: Randomly oriented results for the (a) 1%, (b) 2%, and (c) 4% fiber specimens as well as their averages.

linear increase from the 1% to the 2% specimen across both the spaced and unspaced specimens.

Sample 11 is the cross-layered specimen. We observe that μ_s is approximately twice as large when the steel fibers are top of the layer (closest to our sensor). This suggests that μ_s is more sensitive to nearby fiber percentages. However, we also see a much larger anisotropy factor η (and a larger maximum inductance relative to μ_s) when the 1 percent layer is on top. This suggests the lower layers still affect

Table 1
Table showing anisotropic quantification of each sample

Sample	Percent	Preferentially Aligned	Spaced	μ_s	η	w	ϕ	R^2
1	1	no	N/A	83.6	0.181	0.0334	-21.22	0.9134
2	1	no	N/A	101.7	0.179	0.0359	155.11	0.9458
3	2	no	N/A	196.9	0.169	0.0345	-84.76	0.9537
4	2	no	N/A	190.2	0.084	0.0360	117.24	0.7868
5	4	no	N/A	353.8	0.175	0.0350	6.53	0.9806
6	4	no	N/A	403.9	0.148	0.0345	164.09	0.9745
7	1	yes	yes	217.5	0.671	0.0348	-5.31	0.9851
8	1	yes	no	253.8	0.510	0.0349	-2.22	0.9940
9	2	yes	yes	241.0	0.515	0.0345	-2.95	0.9829
10	2	yes	no	464.8	0.408	0.0342	-10.36	0.9940
11	2 (top) / 1 (bottom)	yes (two orthogonal directions)	yes	280.6	0.190	0.0356	12.14	0.9612
11	1 (top) / 2 (bottom)	yes (two orthogonal directions)	yes	168.7	0.329	0.0357	-173.72	0.9593

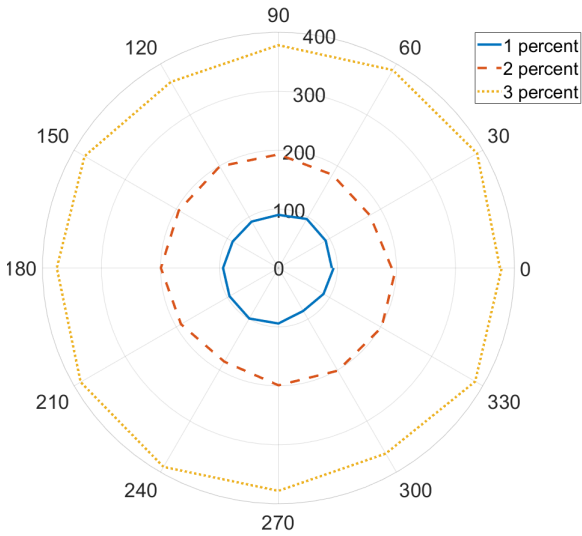


Figure 10: Inductance change (radius) for the Randomly oriented specimens plotted against the different angles. The increase in fiber percentage shows a corresponding increase in the inductance change.

our measurements.

In terms of fit with our theoretical models, all but one demonstrate a good fit (i.e., $R^2 > 0.9$). Based on the data, Sample 4 has a poor fit because of some inherent anisotropy in the sample that might not have been generalized in our theoretical model. The overall average R^2 value across our samples is 0.95. If we remove Sample 4 as an outlier, the average R^2 improves to 0.97. Overall, these results show that our methods can successfully quantify anisotropy in steel fiber reinforced specimen, caused by the variability of the permeability μ values.

In the context of non-destructively testing certain materials, such as UHPC, we often want to determine locations with a high degree of anisotropy or small numbers of fibers. These regions will have different strength properties and may form due to incorrect fabrication practices. This work shows that we can use the estimated specimen permeability and anisotropic factor to identify these two properties.

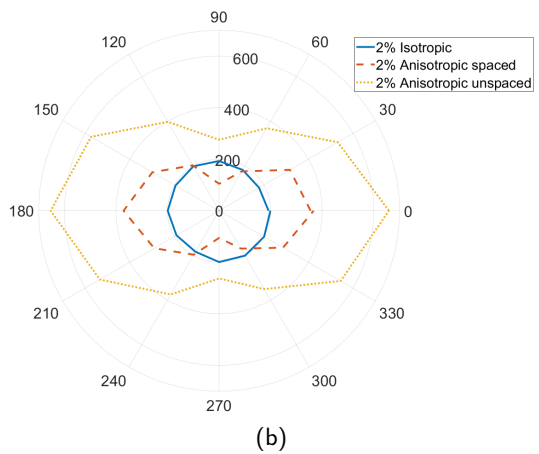
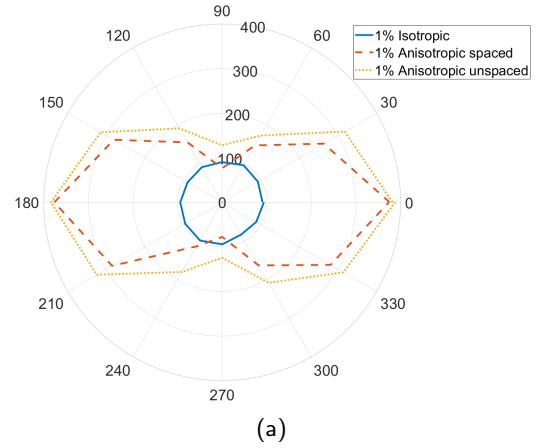


Figure 11: Randomly oriented compared with the preferentially oriented spaced and unspaced results for (a) 1% and (b) 2% specimens.

6. Conclusion

In this work, we were able to show that the electromagnetic method can be used to characterize anisotropy using the inductance method. We also showed that the method outlined in this work can quantify the anisotropy of steel fibers

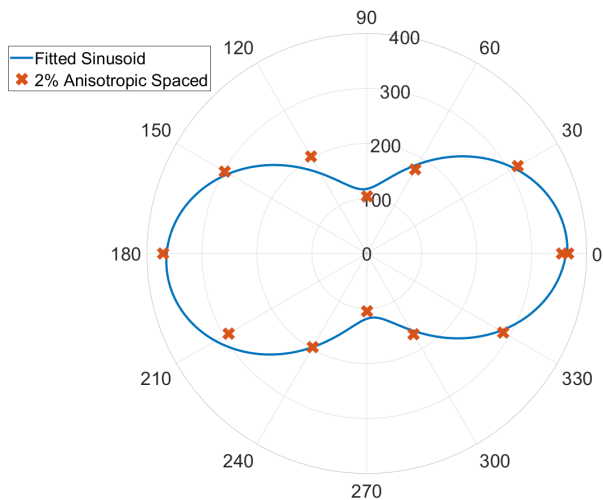


Figure 12: The result of fitting a sinusoid to the plotted points for the 2% preferentially oriented spaced specimen.

within a non-ferromagnetic medium. However, it must be clarified that this method is not applicable when the medium is ferromagnetic or if it contains non-ferromagnetic reinforcement materials, such as glass or nylon.

Also note that a number of simplifying approximations have been carried out by neglecting principally field fringing effects and the non-uniform field distribution in the tested specimen. For a more comprehensive analysis, these effects should be properly modeled via a rigorous solution of the field problem by accounting for the precise geometry. This can be accomplished either by using numerical tools like generic finite elements codes either by semi-analytical approach [33] or resorting to hybrid numerical/spectral approaches [34], when computational speed is required. Non-linear effects, can also be a source of deviation from the expected behaviour, when the exciting field increases, and in this case should be also included in the simulation [35],[36].

7. Acknowledgement

This material is based upon research supported by the Chateaubriand Fellowship of the Office for Science & Technology of the Embassy of France in the United States. We would like to thank CEA, LIST, at Paris-Saclay University, where part of this research has been carried out.

CRedit authorship contribution statement

DJ Alabi: Experimental design, Conceptualization of study, Experimentation, Data Analysis, Manuscript write-up. **A Skarlatos:** Conceptualization of this study, Experimental design, Manuscript write-up and Editing, Supervision. **KA Riding:** Supervision. **C Reboud:** Conceptualization of study, Supervision. **JB Harley:** Conceptualization of study, Data Analysis, Manuscript write-up and Editing, Supervision.

References

- [1] A. Le Hoang, E. Fehling, Influence of steel fiber content and aspect ratio on the uniaxial tensile and compressive behavior of ultra high performance concrete, *Construction and Building Materials* 153 (2017) 790–806.
- [2] A. Hassan, S. Jones, Non-destructive testing of ultra high performance fibre reinforced concrete (UHPC): A feasibility study for using ultrasonic and resonant frequency testing techniques, *Construction and Building Materials* 35 (2012) 361–367.
- [3] W. Meng, M. Valipour, K. H. Khayat, Optimization and performance of cost-effective ultra-high performance concrete, *Materials and Structures/Materiaux et Constructions* 50 (2017).
- [4] M. M. Reda, N. G. Shrive, J. E. Gillott, Microstructural investigation of innovative UHPC, *Cement and Concrete Research* 29 (1999) 323–329.
- [5] S. J. Barnett, J.-F. Lataste, T. Parry, S. G. Millard, M. N. Soutsos, Assessment of fibre orientation in ultra high performance fibre reinforced concrete and its effect on flexural strength, *Materials and Structures* 43 (2010) 1009–1023.
- [6] J. M. Torrents, A. Blanco, P. Pujadas, A. Aguado, P. Juan-García, M. A. Sánchez-Moragues, Inductive method for assessing the amount and orientation of steel fibers in concrete, *Materials and Structures* 45 (2012) 1577–1592.
- [7] D. McCann, M. Forde, Review of NDT methods in the assessment of concrete and masonry structures, *NDT & E International* 34 (2001) 71–84.
- [8] T. Ruan, A. Poursae, Fiber-Distribution Assessment in Steel Fiber-Reinforced UHPC Using Conventional Imaging, X-Ray CT Scan, and Concrete Electrical Conductivity, *Journal of Materials in Civil Engineering* 31 (2019) 04019133.
- [9] L. Mohana Kumar, C. Zeng, S. J. Foster, A stereological approach to estimation of fibre distribution in concrete, *Construction and Building Materials* 324 (2022) 126547.
- [10] A. McNab, M. Campbell, Ultrasonic phased arrays for nondestructive testing, *NDT International* 20 (1987) 333–337.
- [11] G. Karaïskos, A. Deraemaeker, D. G. Aggelis, D. V. Hemelrijck, Monitoring of concrete structures using the ultrasonic pulse velocity method, *Smart Materials and Structures* 24 (2015) 113001.
- [12] M. A. Kewalramani, R. Gupta, Concrete compressive strength prediction using ultrasonic pulse velocity through artificial neural networks, *Automation in Construction* 15 (2006) 374–379.
- [13] J. Hola, K. Schabowicz, State-of-the-art non-destructive methods for diagnostic testing of building structures – anticipated development trends, *Archives of Civil and Mechanical Engineering* 10 (2012) 5–18.
- [14] H. Hu, X. Zhu, C. Wang, L. Zhang, X. Li, S. Lee, Z. Huang, R. Chen, Z. Chen, C. Wang, Y. Gu, Y. Chen, Y. Lei, T. Zhang, N. Kim, Y. Guo, Y. Teng, W. Zhou, Y. Li, A. Nomoto, S. Sternini, Q. Zhou, M. Pharr, F. L. di Scalea, S. Xu, Stretchable ultrasonic transducer arrays for three-dimensional imaging on complex surfaces, *Science Advances* 4 (2018) eaar3979.
- [15] K. Karhunen, A. Seppänen, A. Lehtikoinen, P. J. Monteiro, J. P. Kaijio, Electrical Resistance Tomography imaging of concrete, *Cement and Concrete Research* 40 (2010) 137–145.
- [16] Kobaka, Katzer, Ponikiewski, A Combined Electromagnetic Induction and Radar-Based Test for Quality Control of Steel Fibre Reinforced Concrete, *Materials* 12 (2019) 3507.
- [17] D. J. Daniels, Ground Penetrating Radar, in: *Encyclopedia of RF and Microwave Engineering*, John Wiley & Sons, Inc., Hoboken, NJ, USA, 2005.
- [18] P. Ripka, A. Lewis, Eddy current metal detectors - pulse vs. CW, *Journal of Electrical Engineering* 57 (2006) 175–177.
- [19] J. Svatoš, Single-tone and polyharmonic eddy current metal detection and Non-Destructive testing education software, *J. Phys. Conf. Ser.* 772 (2016) 012052.
- [20] A. N. AbdAlla, M. A. Faraj, F. Samsuri, D. Rifai, K. Ali, Y. Al-Douri, Challenges in improving the performance of eddy current testing: Review, 2019.

- [21] M. Faifer, L. Ferrara, R. Ottoboni, S. Toscani, Low Frequency Electrical and Magnetic Methods for Non-Destructive Analysis of Fiber Dispersion in Fiber Reinforced Cementitious Composites: An Overview, *Sensors* 2013, Vol. 13, Pages 1300-1318 13 (2013) 1300–1318.
- [22] S. I. Babic, C. Akyel, Calculating mutual inductance between circular coils with inclined axes in air, *IEEE Transactions on Magnetics* 44 (2008) 1743–1750.
- [23] M. Faifer, R. Ottoboni, S. Toscani, L. Ferrara, Nondestructive Testing of Steel-Fiber-Reinforced Concrete Using a Magnetic Approach, *IEEE Transactions on Instrumentation and Measurement* 60 (2011) 1709–1717.
- [24] T. Oesch, E. Landis, D. Kuchma, A methodology for quantifying the impact of casting procedure on anisotropy in fiber-reinforced concrete using X-ray CT, *Materials and Structures/Materiaux et Constructions* 51 (2018).
- [25] D. J. Alabi, M. Voss, C. C. Ferraro, K. Riding, J. B. Harley, Electromagnetic method field test for characterizing steel fibers in ultra-high performance concrete (UHPC), *Construction and Building Materials* 374 (2023).
- [26] T. Lei, R. Ottoboni, M. Faifer, S. Toscani, L. Ferrara, A Cost-Effective Method to Assess the Fiber Content and Orientation in Steel Fiber Reinforced Concrete, in: *2019 IEEE International Instrumentation and Measurement Technology Conference (I2MTC)*, IEEE, 2019, pp. 1–6.
- [27] T. S. Oesch, E. N. Landis, D. A. Kuchma, Conventional Concrete and UHPC Performance–Damage Relationships Identified Using Computed Tomography, *Journal of Engineering Mechanics* 142 (2016) 04016101.
- [28] M. Faifer, R. Ottoboni, S. Toscani, A compensated magnetic probe for steel fiber reinforced concrete monitoring, *Proceedings of IEEE Sensors* (2010) 698–703.
- [29] J. A. Stratton, *Electromagnetic theory*, 2007.
- [30] A. K. Bastola, M. Paudel, L. Li, Magnetic circuit analysis to obtain the magnetic permeability of magnetorheological elastomers, *Journal of Intelligent Material Systems and Structures* 29 (2018) 2946–2953.
- [31] D. Alabi, M. Voss, R. Alrashidi, C. Ferraro, K. Riding, J. Harley, Electromagnetic sensor for the nondestructive testing of ultra-high performance concrete (uhpc), *ACI Special Publication on Developments, Applications, and Case Studies in UHPC for Bridges and Structures* (In Press).
- [32] Y. Li, G. Y. Tian, S. Ward, Numerical simulation on magnetic flux leakage evaluation at high speed, *NDT E Int.* 39 (2006) 367–373.
- [33] S. K. Burke, Eddy-current induction in a uniaxially anisotropic plate, *Journal of Applied Physics* 68 (1998) 3080.
- [34] A. Skarlatos, A Mixed Spatial-Spectral Eddy-Current Formulation for Pieces with One Symmetry Axis, *IEEE Transactions on Magnetics* 56 (2020).
- [35] A. Skarlatos, T. Theodoulidis, A Modal Approach for the Solution of the Non-Linear Induction Problem in Ferromagnetic Media, *IEEE Transactions on Magnetics* 52 (2016).
- [36] A. Skarlatos, T. Theodoulidis, Study of the non-linear eddy-current response in a ferromagnetic plate: Theoretical analysis for the 2D case, *NDT & E International* 93 (2018) 150–156.